Supplemental Material: Strong in-plane anisotropy in the electronic structure of fixed-valence β-$LuAlB_4$

Pascal Reiss,[1,2,*] Jordan Baglo,[1,†] Hong'En Tan,[1,3] Xiaoye Chen,[1] Sven Friedemann,[4] Kentaro Kuga,[5,‡] F. Malte Grosche,[1] Satoru Nakatsuji,[5,6,7,8] and Michael Sutherland[1,§]

[1] *Cavendish Laboratory, University of Cambridge, Cambridge, CB3 0HE, United Kingdom*
[2] *Clarendon Laboratory, University of Oxford, Oxford, OX1 3PU, United Kingdom*
[3] *Complex Systems Group, Institute of High Performance Computing, A*STAR, Singapore, 138632*
[4] *HH Wills Laboratory, University of Bristol, Bristol, BS8 1TL, United Kingdom*
[5] *Institute for Solid State Physics, University of Tokyo, Kashiwa 277-8581, Japan*
[6] *CREST, Japan Science and Technology Agency, Kawaguchi, Saitama 332-0012, Japan*
[7] *Department of Physics, University of Tokyo, Bunkyo-ku, Tokyo 113-0033, Japan*
[8] *Trans-scale Quantum Science Institute, University of Tokyo, Bunkyo-ku, Tokyo 113-0033, Japan*

(Dated: July 10, 2020)

Quantum Oscillation Analysis

During the experiment, different field sweep rates and excitation currents were tested to distinguish quantum oscillation signals from other parasitic signals. For the analysis, a low-order polynomial fit to the sample resistance measured as a function of magnetic field was removed from the raw data, carefully chosen not to interfere with the lowest frequencies detected. Quantum oscillation frequencies were mostly extracted directly from a power spectrum using an FFT. Peaks in the FFT were identified when they exceeded the (frequency-dependent) background noise level by at least a factor of two at the lowest temperature measured. The background noise level was estimated from several frequency ranges with no discernible peak, independently for each orientation.

The lowest frequencies below $\approx 0.2\,\mathrm{kT}$ were obtained by fitting the full Lifshitz-Kosevich formula for the resistivity to the background subtracted data [1]. In Fig. SM1, we demonstrate a simultaneous fit to the data as a function of field and temperature, which allows us to extract the frequency, cyclotron mass, and the mean-free path length at the same time.

We briefly comment on the identification of harmonics. As mentioned in the main text, the line 2δ has almost exactly double the frequency compared to δ, and as shown in Fig. SM2(a), the masses extracted for $H||(010)$ equally share that ratio. We therefore identify 2δ as a harmonic of δ. Additional harmonic relations can be identified for the branches β_{4-6} as shown in Fig. SM3.

In Table SMI, we summarise the extracted and computed frequencies and masses for a number of orbits, as well as their mass enhancement compared to DFT where an assignment was possible. Mean-free-path lengths as extracted from the Dingle analysis (Fig. SM2(b)) and the associated quasiparticle mobilities are given where a dominant frequency could be followed over a wide field range, or where direct fits were performed.

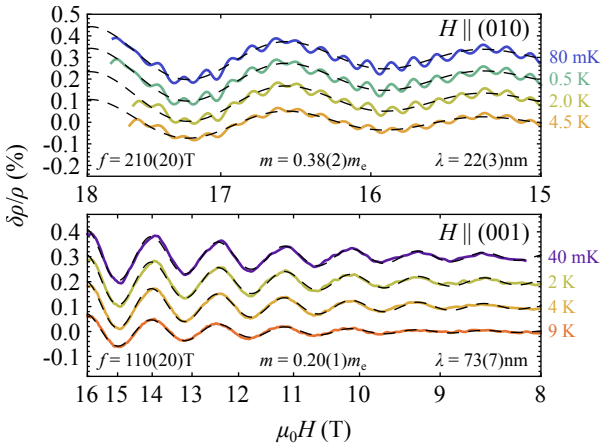

FIG. SM1. Fits of the full Lifshitz-Kosevich form to the background-removed data, simultaneously for several temperatures. The oscillation frequency, the cyclotron mass, and the mean-free path are extracted at the same time.

Effect of Boron Ring and Lattice Variations

In Figure SM4 we present DFT predictions for the charge carrier density in the Lu/Al layer of the unit cell as a function of boron ring variation and the lattice structure. Figure SM4(a) shows the same density as in Fig. 4(b) in the main paper, using experimental lattice parameters for β-$LuAlB_4$, as well as the experimentally determined structure of the boron ring [2]. Figure SM4(b) shows the result for the same overall crystal structure as in β-$LuAlB_4$, but the boron ring is replaced by the one found in β-$YbAlB_4$. Next, in Fig. SM4(c), the boron ring has been replaced by an artificial 'ideal' boron ring. Here, the Lu atom is kept at is experimental site [2], but the B-Lu-B angles are changed to $2\pi/7$. In this case, the B positions and the Lu-B bond lengths are fully determined by keeping the B1 atoms at their high symmetry position $y_{\mathrm{B1}} = 0$. This yields a radius of $r = 2.703\,\text{Å}$ which is slightly larger than the average experimental radii for β-$LuAlB_4$ ($r = 2.694\,\text{Å}$) and

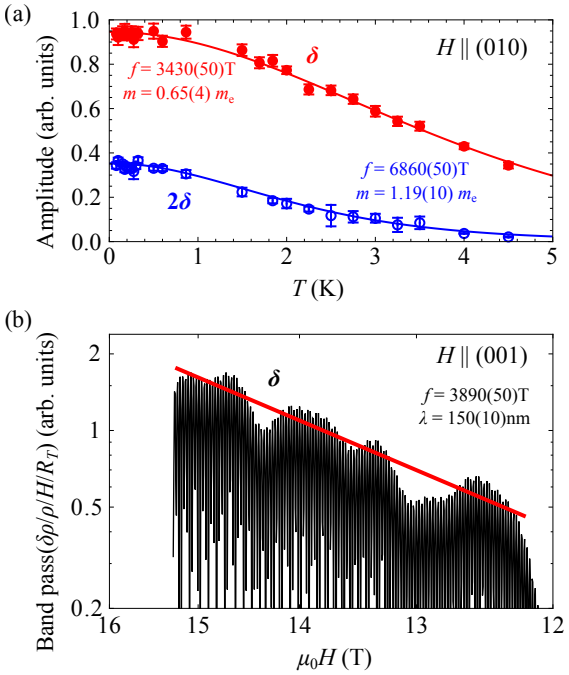

FIG. SM2. (a) Temperature dependence of the amplitude of oscillations δ and 2δ. The integer ratio of the frequencies and cyclotron masses allow us to identify 2δ as a harmonic of δ. (b) Dingle plot of frequency δ to extract the mean free path length.

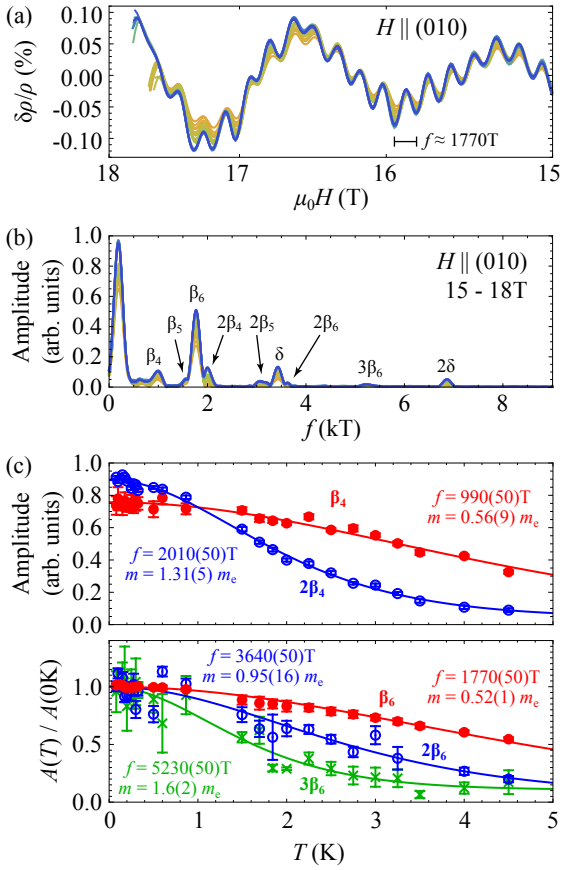

FIG. SM3. (a) Background subtracted data, (b) FFT and (c) mass / harmonic analysis for the field orientation $H||(010)$ showing the origin of the branches β.

β-$YbAlB_4$ (r = 2.696 Å) because the B3 atoms are significantly pushed away from Lu. Finally, in Fig. SM4(d), the lattice and the ring of β-$YbAlB_4$ have been used, but keeping the Lu atom. This effectively corresponds to the setup to determine the 'small' Fermi surface configuration for β-$YbAlB_4$.

Comparing Fig. SM4(a)-(d), the changes in the charge carrier density are minute. In particular, the high-density structure Lu-B3-B3-Lu remains present in the center of the unit cell for all configurations, as do the low-density stripes Al-B2-B2-Al. Focussing on the immediate environment of the Lu atom, Fig. SM4(e) and (f) show the angular dependence of the in-plane charge carrier density surrounding the Lu atom at a distance r, corresponding to half the Lu-B3 bond length for the idealized case, as shown in Fig. SM4(c). Evidently, the charge carrier density is the largest between Lu and B3 for all lattice and ring structures studied, exceeding the densities towards the B1 and B2 sites by an average of 60 %. Most importantly, the relative density variations of cases (a) and (d) are rather similar, while the idealized ring shows the least but still a significant variation.

We conclude therefore that the overall crystal structure plays a very important, possibly even dominant role, in inducing an anisotropic charge density distribution, and thus an anisotropic Lu-B hybridization. The stability of this anisotropy against B ring and lattice structure variations supports our main finding that the underlying electronic structure in β-$YbAlB_4$ should be subject to the same anisotropy as β-$LuAlB_4$.

* pascal.reiss@physics.ox.ac.uk
† Current address: Institut Quantique, Département de Physique & RQMP, Université de Sherbrooke, Sherbrooke, Québec J1K 2R1, Canada
‡ Current address: Toyota Technological Institute, Nagoya, 468-8511, Japan
§ mls41@cam.ac.uk

[1] D. Shoenberg, *Magnetic oscillations in metals* (Cambridge University Press, Cambridge, 1984).
[2] R. T. Macaluso, S. Nakatsuji, K. Kuga, E. L. Thomas, Y. Machida, Y. Maeno, Z. Fisk, and J. Y. Chan, Crystal Structure and Physical Properties of Polymorphs of $LnAlB_4$ (Ln = Yb, Lu), Chemistry of Materials **19**, 1918 (2007).

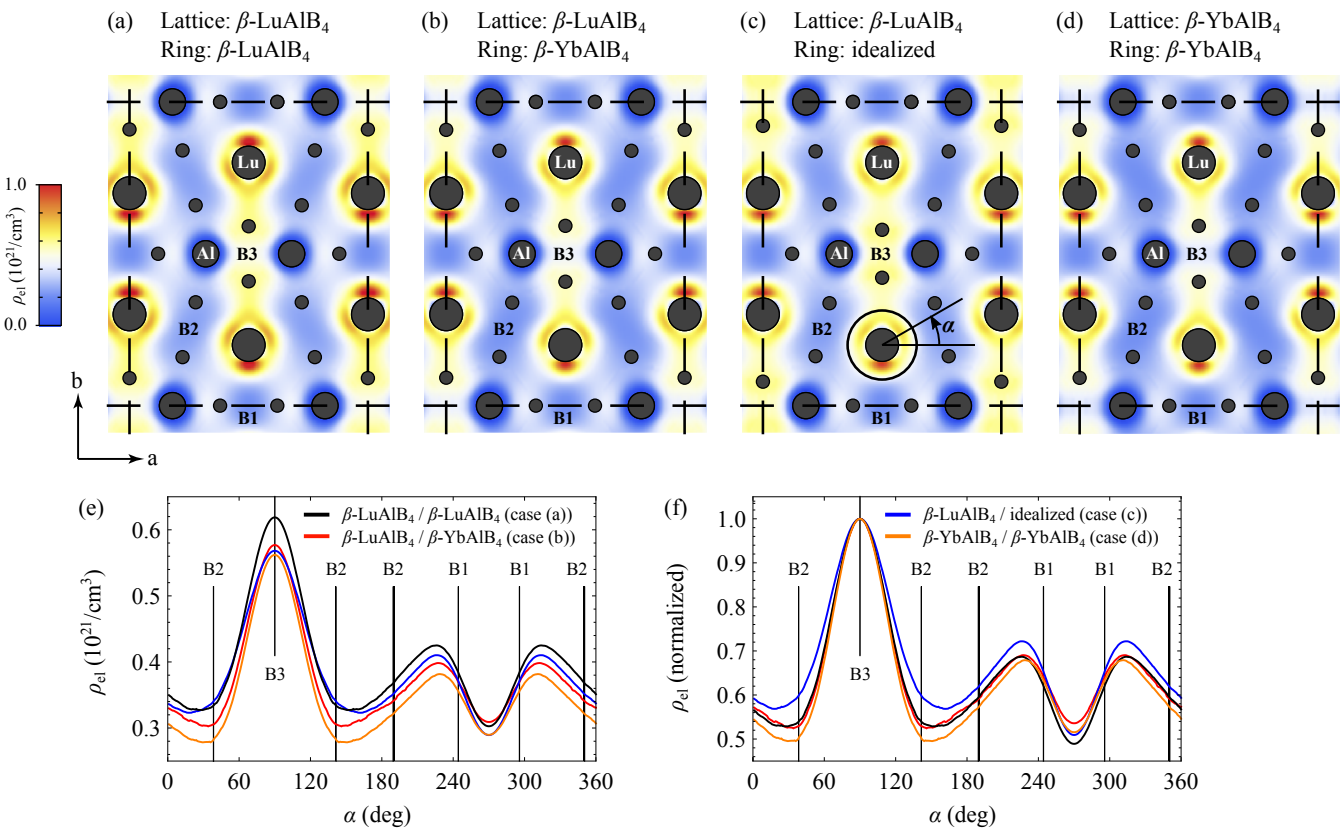

FIG. SM4. Effect of lattice structure and boron ring variation on the charge carrier density in the Lu/Al layer. (a)-(d) Different lattice structure and B ring configurations were used as labelled, and as discussed in the text. (e)-(f) The charge carrier density surrounding the Lu atom at a distance r given by half the Lu-B3 bond length in the idealized case (panel (c)), shown in absolute units (e) and normalised to the peak (f). The vertical lines indicate the directions towards the different B sites.

TABLE SMI. Comparison of experimentally observed orbits (frequencies, cyclotron masses and mean free path lengths/mobilities assuming a circular orbit) with predictions from DFT. An assignment was made where possible. Overall, the mass enhancements vary between 0.5 to 2.1 as expected for the weakly correlated β-$LuAlB_4$. All errors are given as a 1σ confidence interval.

$H||(100)$

Experiment					**DFT**			**Mass**
Orbit	f (T)	m (m_e)	λ (nm)	μ (cm^2/Vs)	Orbit	f (T)	m (m_e)	**enhancement**
γ	64	0.21(2)			γ_1	50	0.10	2.10
					γ_2	70	0.11	1.91
					γ_3	91	0.13	1.62
ϵ	108	0.10(2)			ϵ	113	0.15	0.67
β_6/α_3	480	0.39(2)	44(14)	3100(1000)	α_3	360	0.49	0.80
	550	0.17(3)			β_6	450	0.20	0.85
	2530	—						
β_7 ?	2960	0.44(4)			β_7 (10°)	1940	0.94	0.47
δ	4470	—			δ	4350	0.52	

$H||(001)$

Experiment					**DFT**			**Mass**
Orbit	f (T)	m (m_e)	λ (nm)	μ (cm^2/Vs)	Orbit	f (T)	m (m_e)	**enhancement**
α	111	0.29(2)	73(3)	10800(1500)	α_1	106	0.15	1.93
					α_2	112	0.18	1.61
					α_3	118	0.18	1.61
2α	223	0.60(2)			Harmonics			
3α	335	0.85(8)						
					ϵ	182	0.24	
						232	0.54	
					γ_3	486	0.47	
δ	3890	0.77(8)	150(10)	3700(600)	δ	3850	0.55	1.40
	3930	0.94(7)						1.71
2δ	7840	1.20(1)			Harmonic			

$H||(010)$

Experiment					**DFT**			**Mass**
Orbit	f (T)	m (m_e)	λ (nm)	μ (cm^2/Vs)	Orbit	f (T)	m (m_e)	**enhancement**
						27	0.10	
					β_1	56	0.09	
						76	0.12	
						80	0.11	
ϵ/β_2	110	—			β_2	84	0.10	
					ϵ	154	0.21	
α_3/γ_3	210	0.38(2)	22(3)	2400(400)	α_3	202	0.18	2.11
					γ_3	266	0.32	1.19
β_3/β_4	990	0.56(9)			β_3 (30°)	982	0.51	1.10
					β_4	1250	0.35	1.60
$2\beta_4$	2010	1.31(5)			Harmonic			
β_5	1530	0.73(4)			β_5/β_6	1620	0.42	1.74
β_6	1770	0.52(1)	86(7)	3200(300)				1.24
$2\beta_6$	3640	0.95(16)			Harmonics			
$3\beta_6$	5230	1.6(2)						
δ	3430	0.65(4)	180(20)	4800(700)	δ_1	3110	0.61	1.07(7)
					δ_2	3160	0.55	1.18(7)
2δ	6860	1.19(10)			Harmonic			